APPLIED SCIENCES AND ENGINEERING

Programming a crystalline shape memory polymer network with thermo- and photo-reversible bonds toward a single-component soft robot

Binjie Jin,[1] Huijie Song,[1] Ruiqi Jiang,[2] Jizhou Song,[2] Qian Zhao,[1]* Tao Xie[1]*

The need to support the two most basic functions [three-dimensional (3D)–shaped support and actuation] independently for a typical robot demands that at least two components should be used in its construction. Therefore, component assembly is unavoidable despite the ultimate dream of creating assembly-free robots. We devise a strategy that uses a programmable crystalline shape memory polymer with thermo- and photo-reversible bonds to create a single-component robot. The global 3D-shaped structural support is fabricated via a plasticity-based origami technique enabled by the thermo-reversible bonds. More critically, precisely controlled localized actuation can be programmed into the 3D origami via spatially defined reversible shape memory using the photo-reversible bonds. The overall result is that a polymer thin film can be programmed into various soft robots including a 3D crane and an elephant. Besides reversible shape memory, other types of actuation mechanisms can be potentially introduced via a similar principle. Thus, our strategy represents a general method to create single-component soft robots.

INTRODUCTION

Unlike conventional robots made of metal components, soft material–based robots have demonstrated many unique capabilities (for example, camouflage, perception, and cognition), thus extending their potential utilities into previously unexplored territories (*1*–*9*). Much like conventional robots, however, the functions of these soft robots are also strongly tied to the design (*1*–*9*). From a system standpoint, more than one component is typically needed for robots with functions beyond simple actuation. For instance, a typical robot has a three-dimensional (3D) shape. Within that 3D shape, only certain regions of it have to perform the actuation, whereas the rest provides the static structural support. Therefore, a typical robot should have independent 3D structural support and actuation functions, with the former being static and the latter being active (*1*, *3*, *4*, *7*, *9*). For instance, it was necessary to combine rigid frames (structural support) with soft dielectric elastomers (actuators) to fabricate a functional robotic fish with swimming capability (*9*). To accommodate these two drastically different and potentially interfering functions, sophisticated component assembly is required despite the strong desire to forego such a step. In contrast, we report here a strategy to create a single-component polymeric robot without requiring component assembly. We emphasize that, in the context of this paper, the word "assembly" refers to the macroscopic component assembly, which is different from microscopic molecular assembly as a chemical term. Similarly, the term "component" has a macroscopic meaning that should not be confused with microscopic heterogeneity of polymers. The polymer is a crystalline shape memory network with thermo- and photo-reversible covalent bonds. The thermo-reversible bonds allow the creation of a 3D-shaped structural support via a plasticity-based origami technique (*10*–*12*). Within the same material, photo-reversible bonds can be activated in a spatio-selective manner to create network anisotropy, leading to precisely controlled local actuation via the reversible shape memory mechanism (*13*–*22*). Our concept of origami uni-bot (O-Unibot) is drastically different from a previously reported origami robot for which the origami technique was used to create the robotic body but with the actuation still provided by a conventional motor (*23*). This previous report nevertheless implies the challenge of seamlessly integrating the 3D structure body and actuation within a single component. We further note that other responsive single-component shape-changing 3D structures have been documented in the literature (*10*, *11*, *24*–*28*). However, either their actuation is irreversible (*10*, *11*, *24*, *25*) or the entire 3D structures are intrinsically linked to the reversible actuation (*26*–*28*). In contrast, the advance in this work is that reversible actuation can be spatio-selectively introduced independent of the support structures, which is a key distinction between a reversible actuator and a more sophisticated soft robot.

[1]State Key Laboratory of Chemical Engineering, College of Chemical and Biological Engineering, Zhejiang University, Hangzhou 310027, China. [2]Soft Matter Research Center, Key Laboratory of Soft Machine and Smart Devices of Zhejiang Province, Department of Engineering Mechanics, Zhejiang University, Hangzhou 310027,China.
*Corresponding author. Email: qianzhao@zju.edu.cn (Q.Z.); taoxie@zju.edu.cn (T.X.)

RESULTS

The covalent network containing both thermo- and photo-reversible bonds was synthesized in three steps (Fig. 1A): (i) A four-armed polycaprolactone was prepared by ring-opening polymerization, (ii) the terminal hydroxyl groups were partially modified to form nitro-cinnamates, and (iii) the network was obtained by reacting the unreacted hydroxyl groups with a diisocyanate. An important variable R_c was defined as the ratio between the nitro-cinnamate groups and the original terminal hydroxyl groups, which can be calculated from the ^{1}H nuclear magnetic resonance (NMR) spectra (see fig. S1). Overall, this is a crystalline polyurethane network (melting temperature of 50°C; see fig. S2) with ample esters and cinnamates in the structure. We note that similar chemistry has been widely used in designing polymer networks (*29*–*32*). In particular, the cinnamates are well known to undergo photo-reversible dimerization (Fig. 1B). However, only recent works (*10*, *11*) have revealed that both urethane and ester linkages can be triggered thermally for reversible bond exchanges (Fig. 1B) that are triggered by the same catalyst (dibutyltin dilaurate) used in the network synthesis. Hereafter, we demonstrate that programming via these two sets of noninterfering reversible bonds in a synergistic fashion presents new opportunities to uncover unique shape-morphing behaviors for this otherwise ordinary material.

We first illustrate separately the programming mechanisms via the thermo- and photo-reversible bonds. The thermally induced transesterification and transcarbamoylation trigger the network topological

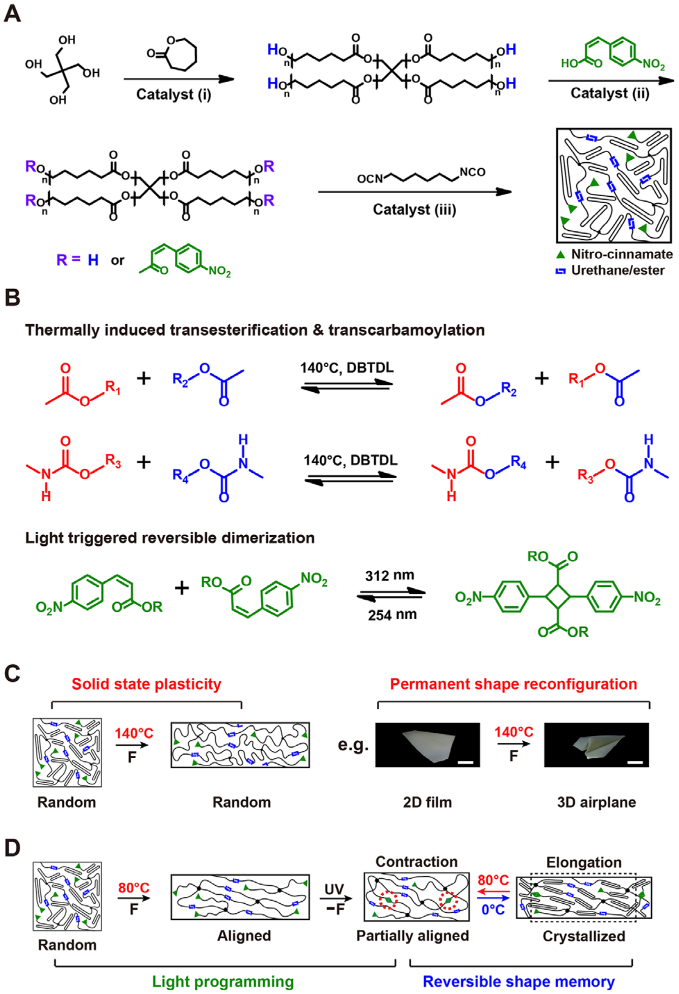

Fig. 1. Network polymer synthesis and programmed shape-morphing mechanisms. (**A**) Synthetic route for the polyurethane network. (**B**) Thermally induced transesterification and transcarbamoylation and photo-reversible dimerization of nitro-cinnamate. (**C**) Mechanisms for permanent shape reconfiguration via solid-state thermal plasticity. (**D**) Reversible actuation via photo-defined reversible shape memory behavior. Scale bars, 1 cm.

rearrangement via dynamic bond exchange (*10*, *11*). Figure 1C shows that the resulting solid-state plasticity allows permanent shape reconfiguration by manual folding (for example, from 2D sheet to 3D airplane) followed by stress relaxation at 140°C. In comparison, Fig. 1D illustrates the process and mechanism for programming the reversible shape actuation using the photo-reversible bonds. The film is first stretched at 80°C, which leads to molecular chain stretching instead of network bond rearrangement because the temperature is sufficiently low and the thermally reversible bonds are not activated. The corresponding strain at this point is defined as the prestretch strain. At the same temperature of 80°C and with the prestretch force still imposed, subsequent exposure to light of 312 nm results in cinnamate dimerization (*29*–*32*), which partially fixes the alignment even after the force is removed. Because of this partial alignment (or network anisotropy), the sample can exhibit an actuation behavior via a reversible shape memory mechanism (*16*–*22*). With the melting and crystallization temperatures of 50° and 18°C, respectively, the sample exhibits crystallization-induced elongation at 0°C and melting-induced contraction at 80°C under a stress-free condition. The orthogonal nature of these two processes permits the independent creation of a 3D shape via plasticity and spatial actuation with photo-induced dimerization. Their combined role toward building 3D soft robots is not known for any existing shape memory polymers.

The reversible shape memory behavior via the mechanism in Fig. 1D can be quantitatively evaluated as the actuation strain, defined as 100% × $(L_{\text{cold}} - L_{\text{hot}})/L_{\text{hot}}$, where L_{cold} and L_{hot} are the sample lengths at 0° and 80°C, respectively. To avoid uneven light penetration, we implemented an experimental protocol that exposes light on both sides of a sample for the same duration for all the samples. Accordingly, each individual curve in Fig. 2A shows that at the same R_c and prestretch strain, the actuation strain increases with the photo-irradiation time and eventually reaches a plateau. Further comparison among the three curves reveals that the plateau irradiation times are similar (80 to 100 s) and the plateau actuation strain increases with R_c. The overall results in Fig. 2A imply that forming more dimer linkages promotes better actuation by longer photo-irradiation (before reaching plateau) and/or having more nitro-cinnamates. This is consistent with the mechanism that the formation of additional photo-induced network points (Fig. 1C) is responsible for the reversible actuation.

Because the reversible actuation originates from crystallization and melting in an anisotropic network (*16*–*22*), the actuation strain is expected to be dependent on the prestretch strain. Figure 2B confirms that the actuation strain increases with the prestretch strain, reaching a saturation level at a prestretch strain of about 400%. We believe that this saturation in actuation strain arises from the stress balance between the stretched network main chains before the irradiation and the nonstretched network main chain formed after dimerization of dangling cinnamates. Overall, the maximum achievable actuation strain under the most optimal conditions is about 40% with excellent stability in cyclic thermomechanical testing (Fig. 2C). This maximum actuation performance is further verified with the photographic images captured in Fig. 2D. The fact that the sample underwent linear elongation/contraction without any noticeable bending proved that light exposure was even. We note that this actuation strain of 40% compares favorably to other reported reversible shape memory polymer systems (*16*–*22*). However, extending the maximum actuation strain further by increasing R_c beyond 0.47 is not feasible because R_c should be kept below 0.50 theoretically to ensure the formation of the polyurethane network before the photo-irradiation. Furthermore, our original motivation for choosing the photo-reversible cinnamate chemistry is twofold: (i) Its nonreactivity under ambient light ensures potential device stability not provided by other types of photo-chemistry such as ultraviolet (UV) curing of acrylates, and (ii) its reversibility may lead to reprogrammability. The actuation performance does not show any noticeable deterioration upon storage for over 1 month. As for the reprogrammability, we found that the actuation can only be partially erased via the photo-reversible reaction and the reprogrammed actuation is lower than the original one (details can be found in fig. S3). Future work may lead to improvement in the reprogrammability, but the goal of the current study is not compromised because of that.

Having optimized the material performance in linear actuation experiments above, we next demonstrate the nonlinear actuations via mask-defined localized photo-irradiation. This is critical because robots often require more complex motions involving various elemental actuation modes beyond simple linear contraction and expansion (*1*–*9*). Here, the choice of photo-patterns can lead to a series of representative

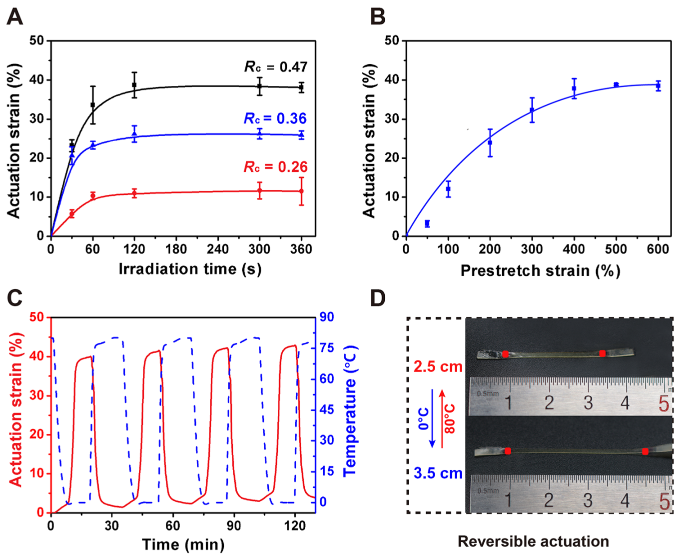

Fig. 2. Quantitative evaluation of the photo-defined reversible actuation. (**A**) Impact of irradiation time and R_c on the actuation strain (prestretch strain is maintained constant at 400%). (**B**) Dependence of actuation strain on prestretch strain (R_c, 0.47; irradiation time, 120 s). (**C**) Cyclic actuation at the maximum actuation strain of 40% (R_c, 0.47; irradiation time, 120 s; prestretch strain, 400%). (**D**) Visual demonstration of the maximum reversible actuation strain of 40% (photo-irradiated active regions are marked in red for better visualization).

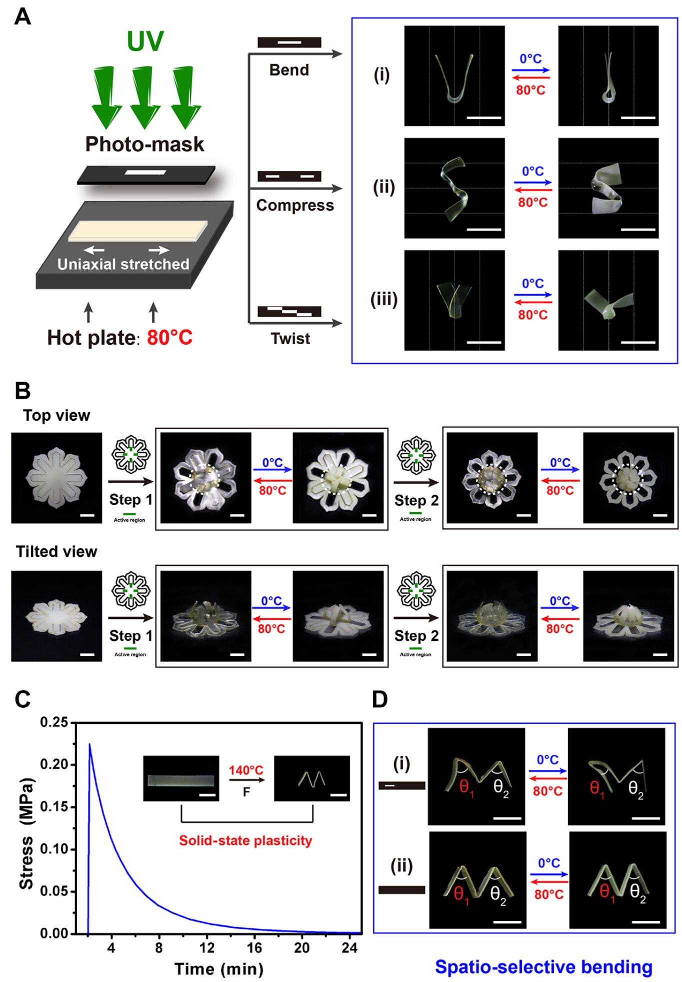

Fig. 3. Demonstration of shape-morphing behaviors via photo-defined reversible actuation and thermally triggered permanent shape reconfiguration. (**A**) Various nonlinear motions realized by localized photo-irradiation. (The white and black colors in the masks denote exposed and unexposed areas, respectively.) (**B**) Sequential programming process of a 3D flower. Green areas represent active regions. (**C**) Stress relaxation curve and construction of a 3D shape via the corresponding solid-state plasticity. (**D**) Spatio-selective actuation in a 3D structure. (i) Selective angular actuation. (ii) No actuation for comparison. Scale bars, 1 cm.

nonlinear actuation modes including bending, compressing, and twisting (Fig. 3A). We note that polymeric actuators, such as liquid crystalline elastomers and hydrogels that can undergo complex 3D actuations, have been reported in the literature (*26*, *28*). Those systems rely on photo-patterning techniques to spatially define material heterogeneities during the material synthesis step, which, for instance, can be cross-linking density for hydrogels (*28*) and topological defect for liquid crystalline elastomers (*26*). In those examples, however, the creation of a 3D shape and actuation are intrinsically linked. Notably, this limitation is applicable to recently emerged examples of reprogrammable liquid crystalline–based reversible actuators (*33*). In contrast, our system has two distinctive advantages: (i) We can decouple the 3D shape versus the actuation, which will be illustrated later in this paper, and (ii) the spatio-selective actuation can be programmed repeatedly in its solid state. Figure 3B shows the sequential programming capability for our system. A 2D film was cut into an eight-petaled flower. Four petals were then selectively programmed to undergo reversible out-of-plane bending in step 1, whereas the other four petals remained inactive. In step 2, the inactive four petals were sequentially programmed to result in all petal actuation.

Besides actuation, robots often have delicate 3D shapes that are tied to their function(s). The solid-state plasticity (*10*–*12*) due to the thermoreversible network bond exchange (Fig. 1C) was first verified in the stress relaxation curve in Fig. 3C. This property can be used to permanently configure a 2D film into a 3D shape such as the "M" shape in Fig. 3C. We now shift our focus to integrate the photo-defined reversible actuation into this M shape. Here, precise control of photo-irradiation on 2D films (all the examples in Fig. 3, A and B) is straightforward, but this is difficult for 3D geometries especially when prestretch is also required. We used the conventional one-way shape memory behavior to overcome this hurdle (*21*), with the corresponding process schematized in fig. S4. Briefly, the 3D M shape was first fixed into a temporary stretched 2D rectangular shape upon which controlled light exposure became feasible. Upon subsequent heat-triggered shape recovery, the stretched 2D rectangular shape reverted back to the M shape with the spatio-selective reversible actuation programmed into it. As a result, the angle θ_1 of M can be selectively programmed to undergo reversible shape change, whereas θ_2 remains unchanged in the same heating and cooling process (Fig. 3D). Without the photo-programming, neither angles in the same M show obvious reversible actuation. We emphasize that more classical reversible shape memory systems can also be programmed from a 2D film into a 3D M shape but only with both angles exhibiting reversible actuations (*16*, *19*, *20*). The type of spatio-selectivity demonstrated here is difficult for those systems (*16*, *19*, *20*) due to the inherent coupling between the programmed actuation and shape. This advantage of our system becomes even more obvious for more sophisticated actuation structures demonstrated hereafter.

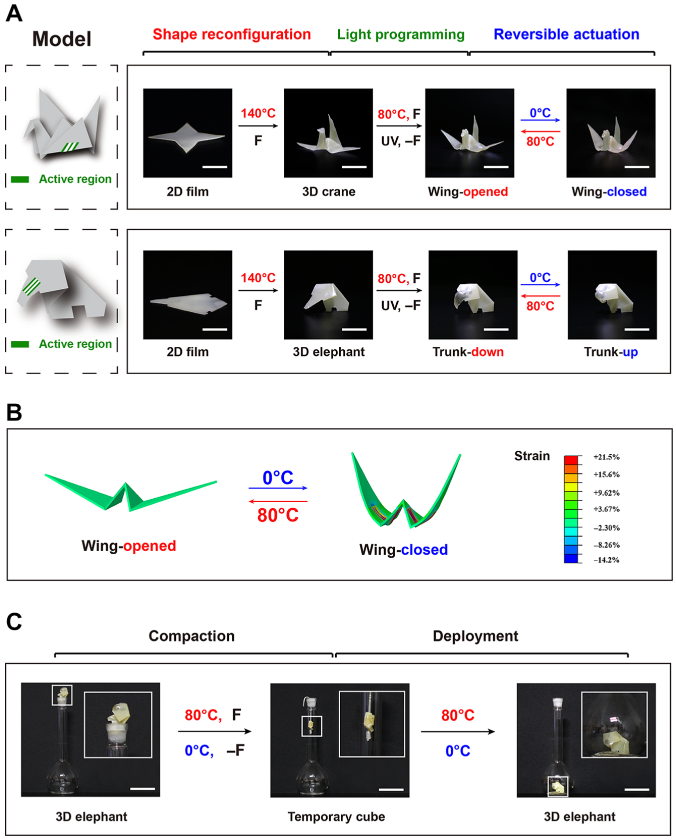

Fig. 4. Single-component O-Unibots. (**A**) Fabrication and reversible actuation of the O-Unibots. (**B**) Finite element simulation of reversible flapping 3D crane. (**C**) Deployment of the O-Unibot via one-way shape memory effect, showing that it cannot enter in the original form but can pass through in the compact temporary form and then deploy back to the robotic form. Scale bars, 1 cm.

The overall results in Fig. 3 set the stage for making more sophisticated O-Unibots. As shown in Fig. 4A, a 2D film was first permanently reconfigured into a 3D crane via the thermally induced plasticity (*10*–*12*). Spatio-selected actuation was then programmed into the active region (highlighted in green in the model) of the 3D crane, yielding reversible wing flapping motions triggered by temperature change. The flapping actions of the crane are captured in movie S1. We note that, to convert the linear elongation/contraction (Fig. 2D) to the reversible bending, only a portion of the wings (the three-strip pattern in the model in Fig. 4A) was activated by light. Thus, the nonactivated surrounding region constrains the reversible bending. Despite such a constraint, the actual reversible strain on the active area is 21.5%, as illustrated with mechanical modeling in Fig. 4B. Without the surrounding constraint, the corresponding reversible strain is 30%. Here, the flapping angle is determined by the mismatch/balance of actuation behaviors between the active and the adjacent inactive regions. Exposure in too large an area would cause undesirable bulging instead of flapping. The three-strip pattern instead of a single strip of a similar area also favors flapping and disfavors bulging. The size and number of strips are limited by the photo-mask we have access to. Overall, the pattern design leads to a notable actuation strain, with room for further improvement if the parameters are optimized in the future. Similarly, an elephant with its trunk showing curling and uncurling actions (reversible actuation) was fabricated, showing the versatility of our approach.

In addition to the reversible actuation, our O-Unibot has the more conventional one-way dual-shape memory behavior. This allows it to be deformed into a compact temporary shape to facilitate its delivery through a narrow pathway and deployed back to the functional robotic form (Fig. 4C). This demonstration in Fig. 4C implies the practical advantages of our O-Unibots for applications such as minimal invasive surgery.

DISCUSSION

The O-Unibot demonstrated above relies on environmental temperature changes for actuation, which inherently limit its speed. On the flip side, its design flexibility is unmatched by any conventional robots. In addition to its ease in fabrication and deployable nature, many attractive functions (for example, surface properties, drug elution capability, and biodegradability) can be potentially introduced given its fully polymeric nature (*21*, *22*). Instead of the passive environmental temperature stimulation, more active stimulation is feasible using, for instance, remote induction or photo-thermal heating (*24*, *27*). Beyond that, considerable opportunities exist in extending the current concept to a variety of other polymeric actuators such as liquid crystalline elastomers (*26*, *27*), hydrogels (*34*), and dielectric elastomers (*9*). This opens up the possibility of designing O-Unibots with suitable performances (for example, speed, strain, and driven mechanisms) to meet diverse practical needs.

MATERIALS AND METHODS

Materials

ε-Caprolactone (ε-CL) (TCI), stannous isooctanoate (TCI), *N,N′*-diisopropylcarbodiimide (TCI), dibutyltin dilaurate (TCI), pentaerythritol (Aladdin), hexamethylene diisocyanate (Aladdin), 4-dimethylaminopyridine (Aladdin), and nitro-cinnamic acid (NCA; Sigma-Aldrich) were all purchased commercially and used as received.

Synthesis of four-armed polycaprolactone (M_n = 10,000)

Polycaprolactone was synthesized by ring-opening polymerization of ε-CL. Pentaerythritol (initiator, 0.1362 g), ε-CL (10 g), and stannous isooctanoate [catalyst, 0.3 wt % (weight %)] were added into a 50-ml flask. The reaction was conducted at 120°C for 10 hours under an argon environment. The obtained polymer was dissolved in toluene and precipitated in cold methanol. The product was then vacuum-dried overnight.

End-group modification of the four-armed polycaprolactone

The degree of end functionalization corresponding to R_c was controlled by the amount of NCA used in the modification reaction. Three samples corresponding to NCA amounts of 1.158, 1.544, and 1.930 g were synthesized. For the general synthesis procedure, weighted NCA was dissolved in 25 ml of *N,N′*-dimethylformamide (DMF) at 50°C. A DMF solution (25 ml) of four-armed PCL (10 g) was added into the NCA solution and stirred for 30 min. *N,N′*-diisopropylcarbodiimide (one molar equivalent to NCA) and 4-dimethylaminopyridine (half a molar equivalent to NCA) were subsequently added, and the mixture was kept at 50°C for 20 hours. The polymer was obtained by precipitation in cold ether. The polymer was redissolved in toluene and reprecipitated in cold ether three times. The final product was obtained by overnight vacuum drying at 40°C.

Synthesis of the polyurethane network

The NCA-functionalized polymer (0.8 g) was first dissolved in DMF (0.8 ml) at 80°C. A butyl acetate solution of the hexamethylene diisocyanate (equimolar based on the remaining end hydroxyl groups) and dibutyltin dilaurate (0.5 wt %) was added into the DMF solution and stirred for several minutes. The liquid mixture was quickly placed between two glass slides (or aluminum plates) separated by a silicone rubber spacer. The precursor solution was kept at 80°C for 48 hours. The obtained film was then vacuum-dried (80°C) overnight.

Permanent shape reconfiguration

Two self-sticking polyimide films were placed on both sides of the polyurethane sample. The trilayered sandwich film was manually folded to form the intended structure and compressed between two glass slides at 140°C for 1 hour. The polyimide films were peeled away, and the remaining polyurethane film was heated at 80°C to yield the new permanent shape.

Programming of the photo-defined reversible actuation

A rectangular sample (12 mm × 3 mm × 0.45 mm) was uniaxially stretched to a target prestrain at 80°C. The film was compressed between two UV transparent silica glass slides to maintain the stretched strain. The assembly was placed on a hot plate (80°C) and exposed to UV light (LED Tao Yuan, 312 nm, 75 mW/cm^2). Both sides of the sample were exposed for the same duration, and the exposure time is defined as the sum of the exposure times for both sides. The actuation programming process was identical for the O-Unibots except that the stretching and compression is applied locally instead of uniformly.

Thermal-mechanical characterization

Reversible actuation strain and thermally induced stress relaxation were both characterized by a dynamic mechanical analysis machine (Q800). The analysis of reversible actuation strain was conducted with cooling/heating cycles between 80° and 0°C (0.01-N pre-load force) in a control force mode. The stress relaxation was conducted at 140°C in a stress relaxation mode.

Finite element simulations

A 3D finite element model was established to simulate the thermomechanical behavior of the reversible shape memory polymer. The anisotropic deformations triggered by temperature were modeled by defining anisotropic thermal expansion coefficients along different directions obtained from the free deformation of shape memory polymer in the experiment. The complex geometry of O-Unibot was developed in SolidWorks and then imported into ABAQUS for thermomechanical analysis. The temperature-dependent modulus was also accounted in the finite element model. As the temperature increased, the different deformations between the active region and the surrounding inactive region induced a strain mismatch, which generated the configuration change of O-Unibot. The parameters used in the simulation were as follows: Young's moduli in the active region, 90.6 MPa (0°C) and 4.06 MPa (80°C); Young's moduli in the adjacent region, 127 MPa (0°C) and 3.47 MPa (80°C); Poisson's ratios were set as 0.48 for both active and adjacent regions; the deformation in the adjacent region due to natural thermal expansion from 0° to 80°C was 0.7%, negligible compared to the deformation in the active region.

SUPPLEMENTARY MATERIALS

Supplementary material for this article is available at http://advances.sciencemag.org/cgi/content/full/4/1/eaao3865/DC1

fig. S1. ^{1}H NMR spectra of the polymer precursors.
fig. S2. Differential scanning calorimeter curve of the polyurethane network.
fig. S3. Cyclic photo-programming and photo-erasing performance.
fig. S4. Scheme for spatio-selective photo-defining reversible actuation onto a 3D shape.
table S1. Photo-programming parameters for locally defined reversible shape memory materials (white area represents the exposed area of the sample).
movie S1. Cyclic reversible actuation of the 3D crane (accelerated by 15).

REFERENCES AND NOTES

1. D. Rus, M. T. Tolley, Design, fabrication and control of soft robots. *Nature* **521**, 467–475 (2015).
2. N. W. Bartlett, M. T. Tolley, J. T. B. Overvelde, J. C. Weaver, B. Mosadegh, K. Bertoldi, G. M. Whitesides, R. J. Wood, A 3D-printed, functionally graded soft robot powered by combustion. *Science* **349**, 161–165 (2015).
3. D. Trivedi, C. D. Rahn, W. M. Kier, I. D. Walker, Soft robotics: Biological inspiration, state of the art, and future research. *Appl. Bionics Biomech.* **5**, 99–117 (2008).
4. S. Kim, C. Laschi, B. Trimmer, Soft robotics: A bioinspired evolution in robotics. *Trends Biotechnol.* **31**, 287–294 (2013).
5. Y. Mengüç, Y.-L. Park, H. Pei, D. Vogt, P. M. Aubin, E. Winchell, L. Fluke, L. Stirling, R. J. Wood, C. J. Walsh, Wearable soft sensing suit for human gait measurement. *Int. J. Robot. Res.* **33**, 1748–1764 (2014).
6. S. A. Morin, R. F. Shepherd, S. W. Kwok, A. A. Stokes, A. Nemiroski, G. M. Whitesides, Camouflage and display for soft machines. *Science* **337**, 828–832 (2012).
7. M. Wehner, R. L. Truby, D. J. Fitzgerald, B. Mosadegh, G. M. Whitesides, J. A. Lewis, R. J. Wood, An integrated design and fabrication strategy for entirely soft, autonomous robots. *Nature* **536**, 451–455 (2016).
8. M. T. Tolley, R. F. Shepherd, B. Mosadegh, K. C. Galloway, M. Wehner, M. Karpelson, R. J. Wood, G. M. Whitesides, A resilient, untethered soft robot. *Soft Robot.* **1**, 213–223 (2014).
9. T. Li, G. Li, Y. Liang, T. Cheng, J. Dai, X. Yang, B. Liu, Z. Zeng, Z. Huang, Y. Luo, T. Xie, W. Yang, Fast-moving soft electronic fish. *Sci. Adv.* **3**, e1602045 (2017).
10. Q. Zhao, W. Zou, Y. Luo, T. Xie, Shape memory polymer network with thermally distinct elasticity and plasticity. *Sci. Adv.* **2**, e1501297 (2016).
11. N. Zheng, Z. Fang, W. Zou, Q. Zhao, T. Xie, Thermoset shape-memory polyurethane with intrinsic plasticity enabled by transcarbamoylation. *Angew. Chem. Int. Ed.* **55**, 11421–11425 (2016).
12. G. Zhang, Q. Zhao, L. Yang, W. Zou, X. Xi, T. Xie, Exploring dynamic equilibrium of Diels–Alder reaction for solid state plasticity in remoldable shape memory polymer network. *ACS Macro Lett.* **5**, 805–808 (2016).
13. T. Chung, A. Romo-Uribe, P. T. Mather, Two-way reversible shape memory in a semicrystalline network. *Macromolecules* **41**, 184–192 (2008).
14. J. Li, W. R. Rodgers, T. Xie, Semi-crystalline two-way shape memory elastomer. *Polymer* **52**, 5320–5325 (2011).
15. Q. Li, J. Zhou, M. Vatankhah-Varnoosfaderani, D. Nykypanchuk, O. Gang, S. S. Sheiko, Advancing reversible shape memory by tuning the polymer network architecture. *Macromolecules* **49**, 1383–1391 (2016).
16. M. Behl, K. Kratz, J. Zotzmann, U. Nöchel, A. Lendlein, Reversible bidirectional shape-memory polymers. *Adv. Mater.* **25**, 4466–4469 (2013).
17. Y. Meng, J. Jiang, M. Anthamatten, Shape actuation via internal stress-induced crystallization of dual-cure networks. *ACS Macro Lett.* **4**, 115–118 (2015).
18. Y. Meng, J.-C. Yang, C. L. Lewis, J. Jiang, M. Anthamatten, Photoinscription of chain anisotropy into polymer networks. *Macromolecules* **49**, 9100–9107 (2016).
19. M. Behl, K. Kratz, U. Noechel, T. Sauter, A. Lendlein, Temperature-memory polymer actuators. *Proc. Natl. Acad. Sci. U.S.A.* **110**, 12555–12559 (2013).
20. J. Zhou, S. A. Turner, S. M. Brosnan, Q. Li, J.-M. Y. Carrillo, D. Nykypanchuk, O. Gang, V. S. Ashby, A. V. Dobrynin, S. S. Sheiko, Shapeshifting: Reversible shape memory in semicrystalline elastomers. *Macromolecules* **47**, 1768–1776 (2014).
21. Q. Zhao, H. J. Qi, T. Xie, Recent progress in shape memory polymer: New behavior, enabling materials, and mechanistic understanding. *Prog. Polym. Sci.* **49–50**, 79–120 (2015).
22. S. A. Turner, J. Zhou, S. S. Sheiko, V. S. Ashby, Switchable micropatterned surface topographies by reversible shape memory. *ACS Appl. Mater. Interfaces* **6**, 8017–8021 (2014).
23. S. Felton, M. Tolley, E. Demaine, D. Rus, R. Wood, A method for building self-folding machines. *Science* **345**, 644–646 (2014).
24. Y. Liu, B. Shaw, M. D. Dickey, J. Genzer, Sequential self-folding of polymer sheets. *Sci. Adv.* **3**, e1602417 (2017).
25. J. Ryu, M. D'Amato, X. Cui, K. N. Long, H. J. Qi, M. L. Dunn, Photo-origami–bending and folding polymers with light. *Appl. Phys. Lett.* **100**, 161908 (2012).
26. T. H. Ware, M. E. McConney, J. J. Wie, V. P. Tondiglia, T. J. White, Voxelated liquid crystal elastomers. *Science* **347**, 982–984 (2015).

27. Y. Yang, Z. Pei, Z. Li, Y. Wei, Y. Ji, Making and remaking dynamic 3D structure by shining light on flat liquid crystalline vitrimer films without a mold. *J. Am. Chem. Soc.* **138**, 2118–2121 (2016).
28. J. Kim, J. A. Hanna, M. Byun, C. D. Santangelo, R. C. Hayward, Designing responsive buckled surfaces by halftone gel lithography. *Science* **335**, 1201–1205 (2012).
29. L. Wang, S. Di, W. Wang, H. Chen, X. Yang, T. Gong, S. Zhou, Tunable temperature memory effect of photo-cross-linked star PCL–PEG networks. *Macromolecules* **47**, 1828–1836 (2014).
30. Y. Zheng, F. M. Andreopoulos, M. Micic, Q. Huo, S. M. Pham, R. M. Leblanc, A novel photoscissile poly (ethylene glycol)-based hydrogel. *Adv. Funct. Mater.* **11**, 37–40 (2001).
31. A. Lendlein, H. Jiang, O. Jünger, R. Langer, Light-induced shape-memory polymers. *Nature* **434**, 879–882 (2005).
32. L. Wu, C. Jin, X. Sun, Synthesis, properties and light-induced shape memory effect of multiblock polyesterurethanes containing biodegradable segments and pendant cinnamamide groups. *Biomacromolecules* **12**, 235–241 (2011).
33. Z. Wang, H. Tian, Q. He, S. Cai, Reprogrammable, reprocessible, and self-healable liquid crystal elastomer with exchangeable disulfide bonds. *ACS Appl. Mater. Interfaces* **9**, 33119–33128 (2017).
34. M. L. Smith, C. Slone, K. Heitfeld, R. A. Vaia, Designed autonomic motion in heterogeneous Belousov–Zhabotinsky (BZ)-gelatin composites by synchronicity. *Adv. Funct. Mater.* **23**, 2835–2842 (2013).

Acknowledgments

Funding: This work was supported by the National Key Basic Research Program of China (no. 2015CB351903), the National Natural Science Foundation of China (nos. 21625402, 21474084, and 51673169), and the Chinese central government's Recruitment Program of Global Experts. **Author contributions:** T.X. and Q.Z. conceived the concept and directed the project. B.J. designed the experiments. B.J. and H.S. conducted the experiments. B.J and T.X. wrote the paper. All authors analyzed and interpreted the data. **Competing interests:** The authors declare that they have no competing interests. **Data and materials availability:** All data needed to evaluate the conclusions in the paper are present in the paper and/or the Supplementary Materials. Additional data related to this paper may be requested from the authors.

Submitted 16 July 2017
Accepted 15 December 2017
Published 26 January 2018
10.1126/sciadv.aao3865

Citation: B. Jin, H. Song, R. Jiang, J. Song, Q. Zhao, T. Xie, Programming a crystalline shape memory polymer network with thermo- and photo-reversible bonds toward a single-component soft robot. *Sci. Adv.* **4**, eaao3865 (2018).

Science Advances

Programming a crystalline shape memory polymer network with thermo- and photo-reversible bonds toward a single-component soft robot

Binjie Jin, Huijie Song, Ruiqi Jiang, Jizhou Song, Qian Zhao, and Tao Xie

Sci. Adv., **4** (1), eaao3865.
DOI: 10.1126/sciadv.aao3865

Science Advances (ISSN 2375-2548) is published by the American Association for the Advancement of Science. 1200 New York Avenue NW, Washington, DC 20005. The title *Science Advances* is a registered trademark of AAAS.